Two-Dimensional Topological Insulator State and Topological Phase Transition in Bilayer Graphene

Zhenhua Qiao, Wang-Kong Tse, Hua Jiang, Yugui Yao, and Qian Niu

Two-Dimensional Topological Insulator State and Topological Phase Transition in Bilayer Graphene

Zhenhua Qiao *,[1] Wang-Kong Tse *,[1] Hua Jiang,[2, 1] Yugui Yao,[3, 1] and Qian Niu[1, 2]

[1]Department of Physics, The University of Texas at Austin, Austin, Texas 78712, USA
[2]International Center for Quantum Materials, Peking University, Beijing 100871, China
[3]Institute of Physics, Chinese Academy of Sciences, Beijing 100190, China

We show that gated bilayer graphene hosts a strong topological insulator (TI) phase in the presence of Rashba spin-orbit (SO) coupling. We find that gated bilayer graphene under preserved time-reversal symmetry is a quantum valley Hall insulator for small Rashba SO coupling λ_R, and transitions to a strong TI when $\lambda_\mathrm{R} > \sqrt{U^2 + t_\perp^2}$, where U and $t_\perp$ are respectively the interlayer potential and tunneling energy. Different from a conventional quantum spin Hall state, the edge modes of our strong TI phase exhibit both spin and valley filtering, and thus share the properties of both quantum spin Hall and quantum valley Hall insulators. The strong TI phase remains robust in the presence of weak graphene intrinsic SO coupling.

PACS numbers: 73.22.Pr,73.43.Cd,75.70.Tj

Recently, there has been a surge of interest in time-reversal invariant topological insulators (TI) [1], a new quantum phase of matter that carries an odd number of helical edge (two-dimensional TIs) or surface (three-dimensional TIs) states. Two-dimensional TI, commonly known as quantum spin Hall (QSH) insulator, occurs in strongly spin-orbit coupled material and was predicted in single-layer graphene with intrinsic spin-orbit (SO) coupling [2] and in HgTe/CdTe quantum well at large well thicknesses [3]. The latter has been confirmed in experiment [4]; graphene, however, has a weak intrinsic SO coupling [5], making it difficult to observe a QSH state. To remedy the situation, a number of recent theoretical [6–10] and experimental [11] work have demonstrated that surface doping on graphene with heavy atoms can dramatically boost the SO coupling strength. Moreover, the broken out-of-plane mirror symmetry creates strong Rashba SO coupling [11], which can induce an interesting quantum anomalous Hall state [7, 8] in the presence of proximity magnetic exchange interaction.

In this Letter, we present a theory of topological phases in gated bilayer graphene in the presence of Rashba SO coupling t_R under preserved time-reversal symmetry. From arguments of band structure and $\mathbb{Z}_2$ topological invariant, we show that this gated bilayer system exhibits two topologically distinct phases, from a quantum valley Hall state at weak t_R to a strong topological insulator state at strong t_R. In a zigzag-edged bilayer system, the strong TI phase has the properties of both quantum valley Hall and quantum spin Hall states. At a fixed t_R, topological phase transition between the two states can be achieved by gate tuning. We also show that the strong TI phase remains robust if weak intrinsic SO coupling is present in addition to the Rashba effect.

The tight-binding Hamiltonian for the AB-stacked bilayer graphene [12] in the presence of Rashba SO coupling and interlayer potential difference (due to an applied gate voltage) is [8, 13]

$$
\begin{aligned}
H_\mathrm{BLG} &= H_\mathrm{SLG}^\mathrm{T} + H_\mathrm{SLG}^\mathrm{B} + t_\perp \sum_{i\in\mathrm{T}, j\in\mathrm{B}, \alpha} c_{i\alpha}^\dagger c_{j\alpha} \\
&\quad + U \sum_{i\in\mathrm{T}, \alpha} c_{i\alpha}^\dagger c_{i\alpha} - U \sum_{i\in\mathrm{B}, \alpha} c_{i\alpha}^\dagger c_{i\alpha},
\end{aligned}
\tag{1}
$$

where the single-layer Hamiltonian $H_\mathrm{SLG}^\mathrm{T,B}$ for the top (T) and bottom (B) graphene layers including Rashba SO coupling [2, 14] is

$$
H_\mathrm{SLG} = t \sum_{\langle ij\rangle\alpha} c_{i\alpha}^\dagger c_{j\alpha} + it_\mathrm{R} \sum_{\langle ij\rangle\alpha\beta} (\boldsymbol{s}_{\alpha\beta}\times\boldsymbol{d}_{ij})_z c_{i\alpha}^\dagger c_{j\beta},
\tag{2}
$$

where $c_{i\alpha}^\dagger$ is the usual creation operator for electron with spin $\alpha = \pm 1$ on site i and t is the intralayer tunneling energy between nearest neighhor sites. The second term on the right-hand side is the Rashba SO interaction with coupling strength t_R, $\boldsymbol{s}$ is the Pauli matrices for the spin degrees of freedom, and $\boldsymbol{d}_{ij}$ is the lattice vector pointing from site j to site i. Interlayer tunneling between the two layers is given by the third term in Eq. (1) with a tunneling energy $t_\perp$, whereas interlayer potential difference $2U$ is given by the last two terms.

We first analyse the bulk band structure obtained from the above Hamiltonian. Figs. 1a-d shows the evolution of the bulk band structure with increasing strength of Rashba SO coupling at fixed interlayer potential difference. In bilayer graphene, a bulk band gap can be opened (panel a) by applying an external gate voltage across the layers [15] to break the inversion symmetry in the out-of-plane direction. When the Fermi level lies within the bulk gap, gated bilayer graphene is a quantum valley Hall (QVH) insulator [8, 16], characterized by a quantized valley Chern number C_v, which is defined as the difference between the Chern numbers at the two valleys K and K'. When the Rashba SO coupling t_R is turned on, we find that the bulk gap decreases gradually with t_R (panel b)
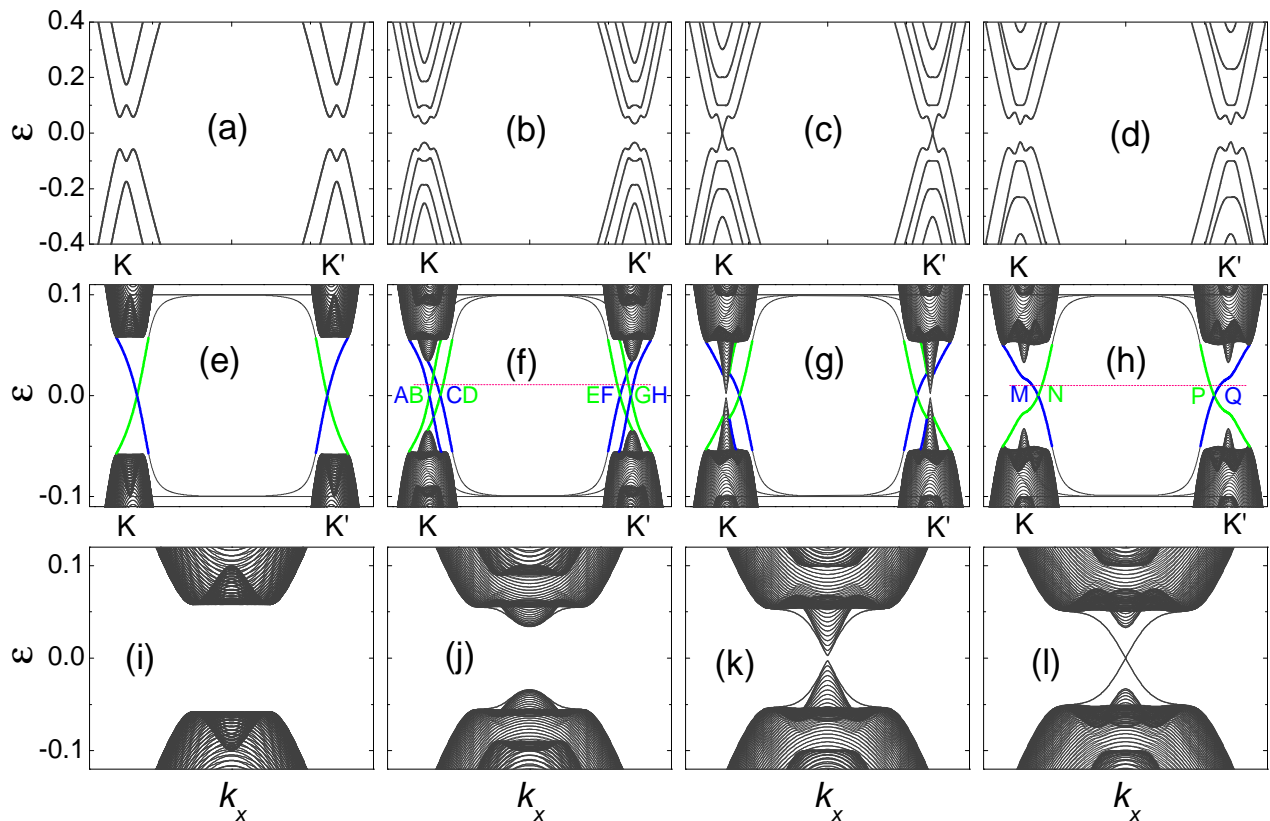
FIG. 1: Evolution of band structure of gated bilayer graphene at a fixed interlayer bias $U/t = 0.1$ for increasing Rashba SO coupling $t_R/t = 0, 0.04, 0.0582, 0.08$. t_R is assumed to be the same on both layers for concreteness. First row (panels a-d): bulk system with periodic boundary conditions; second row (panels e-h): finite strip with zigzag edges; third row (panels i-l): finite strip with armchair edges. In the second row, the dark/blue and light/green curves inside the bulk gap are used to represent edge states located at opposite boundaries. k_x is normalized to inverse lattice constant $1/a$ and the valleys are indicated as K, K'.

and vanishes completely (panel c). Since turning on the Rashba coupling from zero is not accompanied by any band gap closing, it can be inferred that the system remains a QVH insulator at finite t_R and U, before the bulk gap vanishes in panel c. We find that the bulk gap reopens (panel d) when t_R is further increased, and in the vicinity of gap closing the conduction and valance bands cross each other linearly as a function of t_R characteristic of a band inversion. This suggests a topological phase transition, and in the following we show that is indeed so with the emergent phase a two-dimensional strong topological insulator that, interestingly, also possesses the properties of a QVH insulator in the sense that the $\mathbb{Z}_2$ invariant [17] is 1 and the valley Chern number C_v is also 1.

The $\mathbb{Z}_2$ invariant [17] characterizes the band topology in the presence of time-reversal symmetry and is defined by

$$\mathbb{Z}_2 = \frac{1}{2\pi}\left[\oint_{\partial\,\mathrm{HBZ}} \mathrm{d}\boldsymbol{k}\cdot\boldsymbol{A}(\boldsymbol{k}) - \int_{\mathrm{HBZ}} \mathrm{d}^2k\,\Omega_z(\boldsymbol{k})\right]\mathrm{mod}(2),$$

(3)

where $\boldsymbol{A}(\boldsymbol{k}) = i\sum_n\langle u_n(\boldsymbol{k})|\nabla_k u_n(\boldsymbol{k})\rangle$ is the Berry connection summed over all filled band indices n with the periodic part of the Bloch function denoted by $|u_n(\boldsymbol{k})\rangle$, $\Omega_z(\boldsymbol{k}) = (\nabla_k \times \boldsymbol{A})_z$ is the z component of the Berry curvature. By virtue of Kramer's theorem $|u_n(\boldsymbol{k})\rangle$ satisfies the time-reversal invariant constraint $|u_n(-\boldsymbol{k})\rangle = \Theta|u_n(\boldsymbol{k})\rangle$, where Θ is the time-reversal operator. Therefore, we only need to calculate the line and surface integrals in Eq. (3) over half of the Brillouin zone (as denoted by 'HBZ' in the equation) that satisfies the time-reversal constraint. We have computed $\mathbb{Z}_2$ numerically from the Hamiltonian Eq. (1) using the method described in Ref. [18]. Fig. 2 shows our calculated $\mathbb{Z}_2$ phase diagram as a function of U and t_R, where we find that the regimes before and after gap closing are characterized by topologically distinct phases. The system before gap closing is in a QVH phase with a topologically trivial $\mathbb{Z}_2 = 0$ invariant. After gap closing and reopening, we find that $\mathbb{Z}_2 = 1$, therefore proving that the gated bilayer graphene system is a strong TI.

At the topological phase transition critical point, the gap closing condition allows us to obtain an analytic
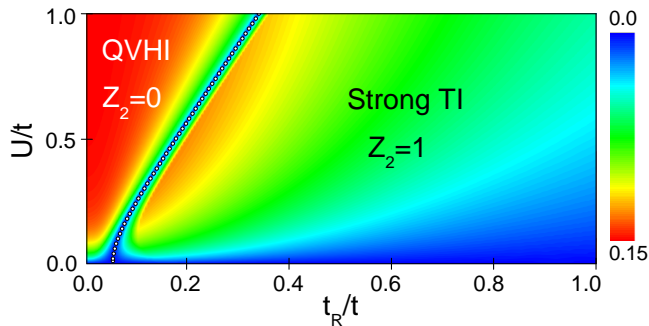
FIG. 2: (Color online) Phase diagram of the $\mathbb{Z}_2$ invariant as a function of U and t_{R} at fixed interlayer tunneling $t_\perp/t = 0.1429$. The color scale represents the magnitude of the bulk gap in units of t. The dotted line plots the phase boundary condition Eq. (5) between the quantum valley Hall insulator (QVHI) and strong TI phases. The bulk gap decreases but remains finite at $U \neq 0$ as t_{R} increases to large values (dark/blue region below the light/green region) in the strong TI phase.

FIG. 3: (Color online) Schematic of edge state propagation in the zigzag edge geometry for (a) QVHI phase at small t_{R}; (b) strong TI state at large t_{R}. The arrows on the edge channels represent in-plane spin directions (out-of-plane spin component is zero). Labels A-H and M-Q correspond to band labels in Figs. 1 f and h.

expression of the phase transition boundary from a low-energy Hamiltonian. Expanding the tight-binding Hamiltonian Eq. (1) in the vicinity of K, K' gives the following eight-band low-energy Hamiltonian

$$H = v(\eta \sigma_x k_x + \sigma_y k_y)\mathbf{1}_s \mathbf{1}_\tau + \frac{t_\perp}{2}(\sigma_x \tau_x - \sigma_y \tau_y)\mathbf{1}_s$$
$$+ \frac{\lambda_{\mathrm{R}}}{2}(\eta \sigma_x s_y - \sigma_y s_x)\mathbf{1}_\tau + U\mathbf{1}_\sigma \mathbf{1}_s \tau_z, \qquad (4)$$

where $\eta = \pm 1$ labels the valley K, K' degrees of freedom, $\boldsymbol{\sigma}$, $\boldsymbol{s}$ and $\boldsymbol{\tau}$ are Pauli matrices representing the A-B sublattice, spin, and layer degrees of freedom, respectively; $\mathbf{1}$ is the identity matrix, the Fermi velocity and Rashba coupling are given respectively by $v = 3ta/2$ and $\lambda_{\mathrm{R}} = 3t_{\mathrm{R}}$. The low-energy Hamiltonian at $k = 0$ gives the energy eigenvalues $\varepsilon = \pm U$ and six other eigenenergies that satisfy the relationship $\varepsilon^3 - \mu U(\varepsilon^2 + \alpha^2 - t_\perp^2 - U^2) - (\alpha^2 + t_\perp^2 + U^2)\varepsilon = 0$ where $\mu = \pm 1$. Imposing the gap closing condition $\varepsilon = 0$ we find the topological phase transition boundary

$$\lambda_{\mathrm{R}}^2 = U^2 + t_\perp^2. \qquad (5)$$

In Fig. 2 we plot Eq. (5) on the $\mathbb{Z}_2$ phase diagram, from which we see that the analytic expression (dotted line) describes accurately the phase transition boundary between the two phases obtained from our numerical $\mathbb{Z}_2$ calculations.

Graphene sheets have two principal edge terminations along and perpendicular to the bond-length direction, respectively known as armchair and zigzag terminations [19]. The valleys K, K' remain good quantum numbers in zigzag-edged strips but are mixed (and hence no longer good quantum numbers) in armchair-edged strips. We first examine the edge band structure in a
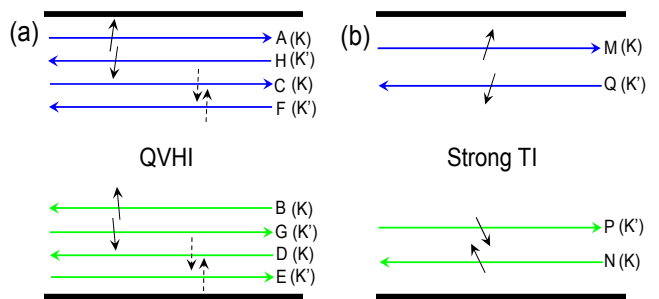
bilayer graphene strip with zigzag edges along one direction and periodic boundary condition along the other direction. Fig. 1e shows the QVH phase at finite U and $t_{\mathrm{R}} = 0$ characterized by a pair of spin-degenerate gapless edge bands. We find that the two valleys are characterized by opposite Chern numbers ± 1, therefore the valley Chern number $\mathcal{C}_{\mathrm{v}} = 2$. With a finite Rashba SO coupling (panel f), the spin degeneracy is lifted yielding two separate pairs of gapless edge bands, and the bilayer system remains a QVH insulator with the same valley Chern number $\mathcal{C}_{\mathrm{v}} = 2$. It can be seen that the outer pair of edge bands (e.g. at valley K, lines labeled A, B) connect the conduction band with the valance band at the same valley, whereas the inner pair of edge bands (e.g. C, D at valley K) connect the two conduction bands or the two valence bands at different valleys. When the bulk gap is closed (panel g), the two pairs of edge bands at each valley merge together with the bulk bands (the upward and downward dips at K and K'); when the bulk gap reopens (panel h) at a larger t_{R}, only one pair of non-degenerate edge states emerges. This change from an even to an odd number of edge states signals a phase transition from a topologically trivial to a topologically nontrivial phase, consistent with our $\mathbb{Z}_2$ calculation. Remarkably, we find that the valley Chern number remains quantized, but changes to $\mathcal{C}_{\mathrm{v}} = 1$. This implies that the strong TI phase is also a QVH insulator and enjoys the same valley protection.

This is illustrated in Fig. 3 showing the edge modes of the QVH and strong TI phases before and after bulk gap closing. At small t_{R}, the QVH phase (Fig. 3a) has two pairs of counterpropagating edge states on each edge that are valley-filtered with different valley quantum numbers K and K'. At large t_{R} after gap reopening the strong TI phase carries only a single pair of counterpropagating edge states. Although the z projections of spins are not good quantum numbers, these counterpropagating edge channels still carry helically opposite spins that are ro-

tated from s_z due to Rashba SO coupling. In the conventional QSH phase [2], the counterpropagating edge states constitutes a Kramer's pair that are spin-filtered. A novel feature in our strong TI phase is that because of valley quantum number conservation, the pair of counterpropagating edge states are *both* spin-filtered and valley-filtered (Fig. 3b), consistent with our bulk topological invariant results $\mathbb{Z}_2 = 1$ and $C_v = 1$. As a consequence, the strong TI phase is topologically protected both by time-reversal symmetry against weak non-magnetic disorder, and by valley-inversion symmetry against weak magnetic disorder that is long-range (longer than lattice spacings) so that intervalley scattering remains prohibited.

For armchair edge geometry, because valleys K and K' overlap and are not good quantum numbers, there is no QVH phase. At finite U and small t_R before phase transition, the system is an ordinary insulator and does not have any gapless edge state (Fig. 1 i - j). When the bulk gap closes and reopens (panels k -l), a single pair of gapless edge states emerges that are not valley-filtered but remain spin-filtered, as expected from a strong TI phase. Unlike the zigzag case however, the armchair case has no valley protection and thus carries a strong TI phase akin to the conventional QSH state.

The predicted TI state in this Letter relies on the presence of a strong Rashba SO coupling, which can be achieved in principle through doping with adatoms [7–9, 11]. This however also enhances the intrinsic SO coupling, and therefore leads to a natural question whether or not the TI state will be destroyed by the presence of intrinsic SO coupling. We address this question by including the intrinsic SO coupling term [20] in each layer of the Hamiltonian Eq. (1). Fig. 4 shows the phase diagram we obtained as a function of both Rashba SO and intrinsic SO coupling strengths at a fixed interlayer potential. First, for small t_R, we find that the QVH phase remains intact when the intrinsic SO coupling t_{ISO} is also small. As t_{ISO} in each layer is increased, the individual-layer quantum spin Hall state due to intrinsic SO coupling prevails, leading to a phase transition to a weak TI phase [21] which is analogous to a layered QSH system. Despite each layer behaves as a QSH state, an even number of such layers renders the overall system topologically trivial that is characterized by a vanishing $\mathbb{Z}_2$ and an even number of gapless edge states. For large values of t_R, we identify a region in the phase diagram where the strong TI phase remains robust. This occurs when the intrinsic SO coupling is about an order of magnitude weaker than the Rashba SO coupling. Indeed, at small values of t_{ISO} the phase diagram remains qualitatively similar to Fig. 2 at $t_{ISO} = 0$, with the only difference that the gapless metallic regime (white region in Fig. 4) between the QVH and strong TI phases becomes more extended.

In conclusion, we have shown that gated bilayer graphene hosts a strong topological insulator phase at
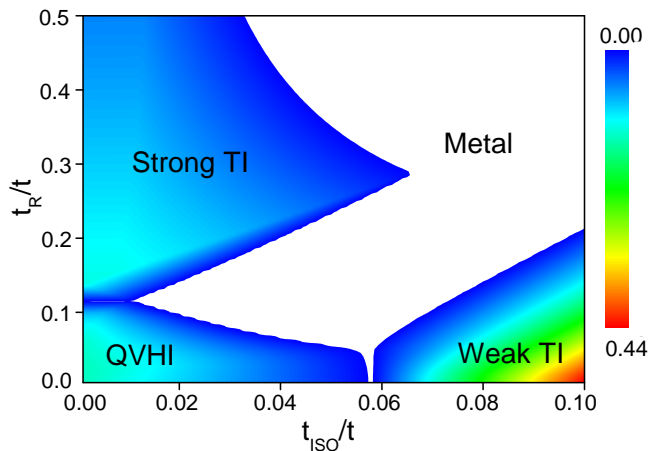

FIG. 4: (Color online) Phase diagram as a function of Rashba t_R and intrinsic t_{ISO} SO coupling strengths (taken to be same on both layers) at finite $U/t = 0.3$. The color scale indicates the magnitude of the bulk gap in units of t. The white region corresponds to a metallic phase where there is no global gap in the bulk band structure.

large Rashba spin-orbit coupling. The gate voltage can serve as a topological switch that tunes between the quantum valley Hall phase and the strong topological insulator phase. This can be realized by enhancing the spin-orbit coupling in graphene through adatom doping.

* These authors contributed equally to this work.

[1] For recent reviews, see M. Z. Hasan and C. L. Kane, Rev. Mod. Phys. **82**, 3045 (2010); X.-L. Qi and S.-C. Zhang, arXiv:1008.2026v1.
[2] C. L. Kane and E. J. Mele, Phys. Rev. Lett. **95**, 226801 (2005).
[3] B. A. Bernevig, T. L. Hughes, and S.-C. Zhang, Science, **314**, 1757 (2006).
[4] M. Koenig *et al.*, Science **318**, 766 (2007).
[5] H. Min *et al.*, Phys. Rev. B **74**, 165310 (2006); Y. G. Yao *et al.*, Phys. Rev. B **75**, 041401(R) (2007); M. Gmitra *et al.*, Phys. Rev. B **80**, 235431 (2009).
[6] A. H. Castro Neto and F. Guinea, Phys. Rev. Lett. **103**, 026804 (2009).
[7] Z. H. Qiao *et al.*, Phys. Rev. B **82**, 161414(R) (2010).
[8] W.-K. Tse *et al.*, Phys. Rev. B **83**, 155447 (2011).
[9] C. Weeks *et al.*, arXiv:1104.3282v1 (2011).
[10] H. Zhang *et al.*, arXiv:1108.5915v1 (2011).
[11] A. Varykhalov *et al.*, Phys. Rev. Lett. **101**, 157601

(2008); Y. S. Dedkov *et al.*, Phys. Rev. Lett. **100**, 107602 (2008); O. Rader *et al.*, Phys. Rev. Lett. **102**, 057602 (2009); A. Varykhalov and O. Rader, Phys. Rev. B **80**, 035437 (2009).

[12] E. McCann and V. I. Falko, Phys. Rev. Lett. **96**, 086805 (2006); J. Nilsson *et al.*, Phys. Rev. B **78**, 045405 (2008).

[13] R. van Gelderen and C. Morais Smith, Phys. Rev. B **81**, 125435 (2010).

[14] R. Winkler and U. Zulicke, Phys. Rev. B **82**, 245313 (2010).

[15] E. V. Castro *et al.*, Phys. Rev. Lett. **99**, 216802 (2007); K. F. Mak *et al.*, Phys. Rev. Lett. **102**, 256405 (2009).

[16] W. Yao, S. A. Yang, and Q. Niu, Phys. Rev. Lett. **102**, 096801 (2009); F. Zhang *et al.*, Phys. Rev. Lett. **106**, 156801 (2011).

[17] C. L. Kane and E. J. Mele, Phys. Rev. Lett. **95**, 146802 (2005); L. Fu and C. L. Kane, Phys. Rev. B **74**, 195312 (2006).

[18] T. Fukui and Y. Hatsugai, J. Phys. Soc. Jpn. **76**, 053702 (2007); A. M. Essin and J. E. Moore, Phys. Rev. B **76**, 165307 (2007); D. Xiao *et al.*, Phys. Rev. Lett. **. 105**, 096404 (2010).

[19] A. H. Castro Neto *et al.*, Rev. Mod. Phys. **81**, 109 (2009).

[20] The graphene intrinsic SO coupling is given by Eq. (6) of Ref. 2 with the same notations as our paper.

[21] E. Prada *et al.*, Solid State Commun. **151**, 1075 (2011).